catalysts

MDPI

Review

Controllable and Large-Scale Synthesis of Carbon Nanostructures: A Review on Bamboo-Like Nanotubes

Zirui Jia [1], Kaichang Kou [1], Ming Qin [2], Hongjing Wu [1,*], Fabrizio Puleo [3] and Leonarda Francesca Liotta [3,*]

1 School of Science, Northwestern Polytechnical University, Xi'an 710072, China; jiazirui@stu.xjtu.edu.cn (Z.J.); koukc@nwpu.edu.cn (K.K.)
2 Faculty of Materials Science and Chemistry, China University of Geosciences, Wuhan 430074, China; qinming@cug.edu.cn
3 Institute for the Study of Nanostructured Materials (ISMN)-CNR, Via Ugo La Malfa 153, 90146 Palermo, Italy; puleo@pa.ismn.cnr.it
* Correspondence: wuhongjing@mail.nwpu.edu.cn (H.W.); leonarda.liotta@ismn.cnr.it (L.F.L.); Tel.: +86-29-8843-1664 (H.W.); +39-91-680-9371 (L.F.L.)

Academic Editors: Di-Jia Liu and Jianguo Liu
Received: 27 July 2017; Accepted: 18 August 2017; Published: 30 August 2017

Abstract: Bamboo-like carbon nanotubes are members of the carbon nanotubes (CNTs) family, whose structure is made up of separated hollow compartments and bamboo knots. Due to the peculiar structure of the CNTs species, the growth mechanism and related features have been widely investigated. Bamboo-like carbon nanotubes are widely applied in several fields, such as sensors, adsorbents, catalysts, and lithium-ion battery electrodes materials. Different methods have been applied for the synthesis of carbon nanotubes, among them, catalytic chemical vapor deposition has been singled out as the most used procedure due to low cost with a high quality product. The present review is devoted to increasing the literature dealing with the design, synthesis, and characterization of bamboo-like carbon nanotubes grown over different catalysts. Results on the methane dry reforming reaction, hydrocarbon thermal decomposition, special chemical vapor deposition as well as other methods applied to the preparation of bamboo-like carbon nanotubes are discussed. The differences in the carbon deposits between the dry reforming reaction and other reaction methods are compared and possible formation mechanisms of bamboo-like carbon nanotubes are discussed.

Keywords: bamboo-like carbon nanotubes; preparation methods; dry reforming reactions; hydrocarbon thermal decomposition; chemical vapor deposition; structural properties; Transmission electron microscopy (TEM) characterization

1. Introduction

In recent years, carbon nanomaterials with different shapes such as carbon nanotubes, nanospheres, nanofibers, and graphene have been widely investigated due to their peculiar properties that are a function of their structure, thus finding in turn applications in different fields [1–3].

Due to their unique spherical structure, porous carbon nanospheres (CNS) can provide a fast molecular diffusion/transfer which is of great importance for their applications [1]. Metal nanoparticles located in the core of the hollow carbon nanospheres enhance the reaction rate and improve the selectivity without deactivation during the reaction. Considering the easy diffusion of electrolytes to carbon surfaces, the carbon nanospheres are also supposed to be promising electrode materials for supercapacitors. Ultrafine carbon nanospheres have been successfully employed for biomedical and pharmaceutical applications, such as drug delivery.

As carbon nanofibers (CNFs), the graphene layers can be perpendicular, inclined or even coiled along the fiber axis. With the variation of the synthesis method, CNFs with different morphological features, such as core/shell structure and hierarchical pores can be obtained. CNFs with the above structure possess excellent electrical properties for application in the field of conductive additives and electrode materials [2]. Carbon nanotubes (CNTs) commonly consist of graphene layers rolled up into a seamless cylinder with the plane parallel to the longitudinal axis. Based on the number of graphitic layers, the CNTs can be classified into single-walled CNTs (SWCNTs) and multiwalled CNTs (MWCNTs). The outstanding physicochemical properties of CNTs including high tensile strength, high electrical conductivity, high ductility, and relative chemical inactivity result in a wide range of application fields, such as energy storage, heterogeneous catalysis, gas storage, sensors, etc. [3]. It is known that the shape and morphology of the nano-scale inorganic materials can be greatly influenced by the synthesis method [4–32]; since the appearance of the landmark paper by Ijima on carbon nanotubes (CNTs) [33], carbon materials with different morphologies have been successfully prepared by several methods, such as chemical vapor deposition (CVD), the hydrothermal process and catalytic decomposition, etc. [34–42]. Although several procedures have been applied for the synthesis of carbon nanotubes, the controllable and selective synthesis of carbon nanomaterials still remains a challenge. Actually, graphene is a relatively new material, which has several advantages such as a three dimensional network, high surface area, high electro/thermo conductivities, high chemical/electrochemical stability, high flexibility and elasticity, and extremely high surface hydrophobicity [43,44].

In this review, we mainly focus on controllable synthesis of traditional carbon nanotubes (CNTs), especially bamboo-like carbon nanotubes. Bamboo-like carbon nanotubes are members of the carbon nanotubes family. Different from the normal CNTs, the structure of bamboo-like carbon nanotubes is made up of separated hollow compartments and bamboo knots which grow straight along the axis. Compared with standard carbon nanotubes, bamboo-like nanotubes possess peculiar properties, such as high specific surface and high density of defects, and in the most recent years have drawn increasing attention [45–71]. The bamboo-like carbon nanotubes are promising adsorbents for the removal of organic pollutants due to their large surface area [72,73]. The excellent hydrogen storage capacity and lithium storage properties have also increased their application for hydrogen storage and lithium-ion battery electrodes [74,75]. Besides, these bamboo-like carbon nanotubes are also components of sensors [76]. The bamboo-like carbon nanotubes can be produced by different routes and their structure has been investigated by scanning electron microscopy (SEM) and transmission electron microscopy/high resolution transmission electron microscopy (TEM/HRTEM) characterizations, as shown in Table 1, where an overview of the used catalysts, reaction conditions, and carbon products is given.

Different methods have been used for the synthesis of carbon nanotubes, such as chemical vapor deposition (CVD) [34], plasma enhanced chemical vapor deposition (PECVD) [62] alcohol catalytic chemical vapor deposition (CCVD) [60], hydrothermal [35] or sonochemical reaction, and high-pressure CO conversion (HiPco) [48].

On the contrary, only a few examples concerning the formation of carbon nanotubes with bamboo-like structure during dry reforming reactions have been cited in the literature [18,54–56].

The present review article reports on the synthesis of bamboo-like nanotubes by using reforming reactions and compares the properties of the so obtained carbon nanostructures with those of bamboo-like carbon nanotubes (CNTs) synthesized by employing other methods, with the aim of giving an overview of the relationship between structure, properties, and synthesis procedures.

The focus of the present work on bamboo-like carbon nanotubes (CNTs) stems from their formation mechanism which is a function of the specific reaction. In dry reforming reactions, the carbon atoms generated on the catalyst surface have different mobility, depending on the nature of the active sites, and assemble into hexagonal and pentagonal rings. The pentagonal carbon rings introduce changes in the curvature of graphitic flake to accommodate the geometry of the interior

layers, thus facilitating the formation of bamboo-like nanotubes [18]. A growth mechanism, involving a jump of the Ni particle followed by the formation of conical holes, occurs for bamboo-like carbon nanotubes (CNTs) formation during the hydrocarbon thermal decomposition process [57], as reported in Section 3.

In this review, the structure and morphology of bamboo-like carbon nanotubes are investigated by SEM and TEM characterizations. Also, we have shown that HRTEM can further provide information about particle size distribution and lattice fringe of the carbon nanotubes and related catalysts [77–89]. The controllable synthesis of carbon nanotubes with tailored properties is certainly a challenge for researchers thanks to their valuable applications in several fields.

Table 1. The synthesis method of bamboo-like carbon nanotubes over different catalysts, their morphological and structural characterization along with the experimental conditions used.

Synthesis Method		Reaction Catalyst	Conditions	Products	Refs.
dry reforming reactions	CH_4 dry reforming	NiAl, NiAlMg, NiAlCe, NiAuAl, NiPtAl, NiAuPtAl, NiAuPtAlMg, NiAuPtAlCe	750 °C, 1 atm pressure, 24 h long run test	9.48 wt % bamboo-like CNTs on NiAuPtAl	[18]
	glycerol dry reforming	Ni/Al_2O_3, 3 wt % $La-Ni/Al_2O_3$, 5 wt % $La-Ni/Al_2O_3$	750 °C, 1 atm pressure	55 wt % and 30 wt % bamboo-like CNTs on Ni/Al_2O_3 and 5 wt % $La-Ni/Al_2O_3$	[55]
hydrocarbon thermal decomposition	methane thermal decomposition	Ni nanoparticles	930 °C, 1 atm pressure	86 wt %~87.5 wt % bamboo-like CNTs on Ni nanoparticles	[57]
		$Ni-Cu/Al_2O_3$	720–770 °C, 1 atm pressure	0.7–33 mg C/mg Ni bamboo-like CNTs on $Ni-Cu/Al_2O_3$	[58]
		Ni and Ni-Cu alloys	750 °C, 1 atm pressure	407 g C/g Ni bamboo-like CNTs on $Ni_{47}Cu_{53}/CNT$	[59]
special chemical vapor deposition	catalytic chemical vapor deposition	$LaNiO_3$ perovskite	800 and 900 °C, 1 atm pressure	68.8 wt % and 49.3 wt % bamboo-like CNTs on $LaNiO_3$	[60]
	detonation-assisted chemical vapor deposition	Ni nanoparticles with the doping of sulfur	900 °C, 40 MPa pressure	high quality bamboo-like CNTs on Ni without S	[61]
	microwave plasma enhanced chemical vapor deposition	thermally oxidized silicon substrates with a platinum thin film catalyst	1000 °C, 2780 Pa pressure	vertically aligned bamboo-like CNTs on Pt film	[62]
pyrolysis and gasification of plastic wastes	pyrolysis of low density polyethylene feedstock	Nickel, iron, cobalt and copper catalysts	800 °C, 1 atm pressure	45.7 mg C/g plastic and ~180 mg C/g plastic bamboo-like CNTs on Ni/Al_2O_3 and Fe/Al_2O_3	[71]

2. Dry Reforming Reactions

The dry reforming reaction for the production of bamboo-like carbon nanotubes over different catalysts was recently reported in several literature examples [18,54–56]. Among the dry reforming reactions, CH_4 dry reforming and glycerol dry reforming are the common routes for the fabrication of bamboo-like carbon nanotubes.

In a previous work, we investigated the nature of carbon deposits grown on Ni-based catalysts for the methane dry reforming (DRM) reaction [18]. In order to have a better understanding of the catalytic differences between the various catalysts, a careful microscopic investigation was performed on the catalysts after long-run tests at 750 °C (Figure 1).

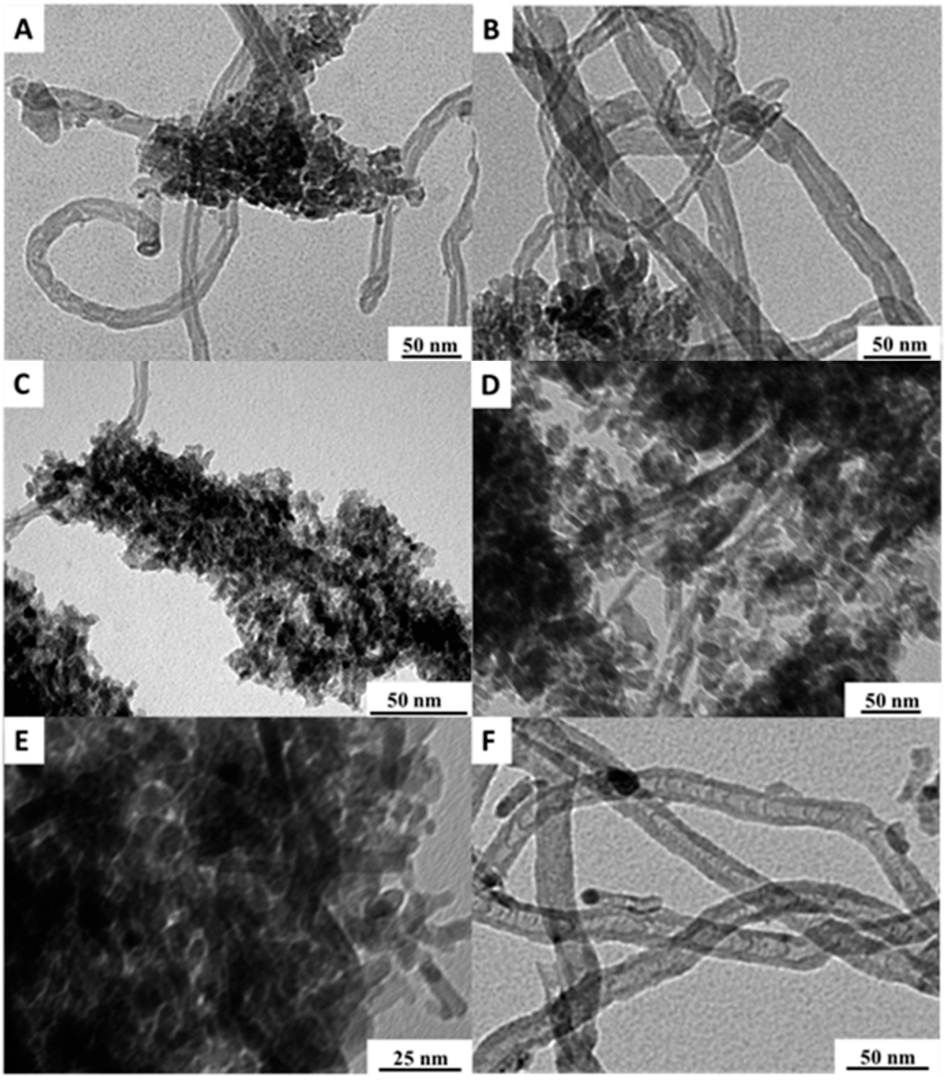

Figure 1. Transmission electron microscopy (TEM) images of selected catalysts after long run (at higher magnification): NiAl (**A**); NiAlCe (**B**); NiAlMg (**C**); NiAuAl (**D**); NiPtAl (**E**); NiAuPtAl (**F**) (reprinted with permission from Ref. [18], copyright 2014 Elsevier).

A first screening performed by means of TEM revealed a clear difference in terms of carbonaceous species present on the surface of the catalysts after the long-run experiments. TEM results revealed that the most active catalysts were those presenting the carbonaceous species in the form of nanotubes on the surface (NiAuPtAl and NiAlCe) (Figure 1B,F respectively). Generally, we observed that the nature of carbon deposits and their relative amount depend on the type of catalyst (active metals and/or support type). In details, for the monometallic NiAl (Figure 1A) catalyst, there are at least two types of carbon (i.e., amorphous carbon and carbon nanotubes). The NiAlMg (Figure 1C) as well as the bimetallic (Ni-Au/Pt) catalysts present a high amount of amorphous carbon. In the case of NiAlCe (Figure 1B) carbonaceous species in the form of nanotubes were also found, while a nice bamboo-like structure was detected for NiAuPtAl (Figure 1F) trimetallic catalyst. From what was observed by microscopic characterization it appears clear that there is a strong correlation between

catalytic activity and the typology/amount of carbonaceous species. The best catalysts are those with the best combination of these two parameters (high amount of carbon nanotubes together with a low quantity of total carbon).

Four kinds of hydrotalcite derived catalysts, i.e., HT-25Ni, HTNi-Ce, HTNi-Zr, and HTNi-CeZr were synthesized by Costa et al. [54] and used for the dry methane reforming reaction at 550 °C. Activity and selectivity of hydrotalcite derived catalysts were investigated. The structure of the carbon deposit on the HT-derived catalysts after 300 min of DRM reaction at 550 °C was studied. TEM images are shown in Figure 2. Carbon deposit on the HT-25Ni and HTNi-Ce catalysts (Figure 2a,b respectively) exhibited a fishbone carbon nanofibers structure, graphite planes with thicknesses ranging from 5 to 20 nm were also observed. In the case of HTNi-Zr and HTNi-CeZr catalysts, (Figure 2c,d respectively) fishbone carbon nanofibers structures were not obtained but instead multi-wall and even single-wall carbon nanotubes. These bamboo-like carbon nanotubes composed of only 1–4 graphite planar layers were thinner than fishbone fibers formed over HT-25Ni and HTNi-Ce catalysts. These results evidenced the role played by Zr on the carbon nanostructures, preventing the formation of fishbone carbon nanofibers during the methane decomposition process.

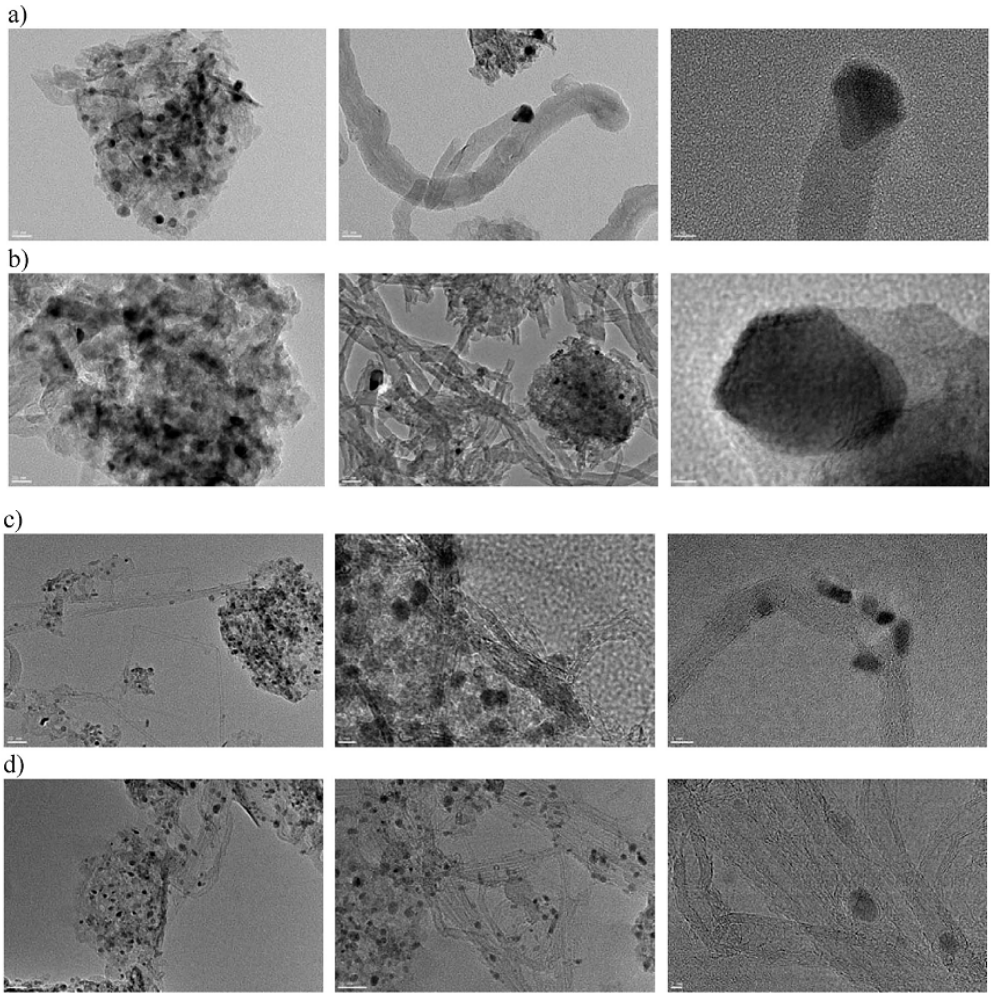

Figure 2. TEM images for (**a**) HT-25Ni; (**b**) HTNi-Ce; (**c**) HTNi-Zr; and (**d**) HTNi-CeZr catalysts after 300 min methane dry reforming (DRM) at 550 °C (reprinted with permission from Ref. [54], copyright 2016 Elsevier).

A long-run stability of La promoted Ni/Al_2O_3 catalysts for glycerol-dry reforming was proposed by Cheng et al. [55]. Field emission scanning electron microscopy (FE-SEM), TEM, and HRTEM analyses of catalysts after 72 h reaction were performed, as shown in Figure 3.

It was shown that that the carbon deposit was composed of graphitic filamentous. After 72 h reaction over Ni/Al_2O_3 catalyst, most of the carbon deposit exhibited a nano-filaments structure whose diameter ranged from 10 to 30 nm as displayed in Figure 3a,b. Bamboo-like carbon nanotubes whose structure was observed by HR-TEM (Figure 3c) were obtained due to carbon bulk diffusion through the catalyst particle surface as discussed previously [56]. Moreover, a carbon deposit with the structure of helical and wavy whisker type thin filaments was obtained after 72 h reaction over the $La\text{-}Ni/Al_2O_3$ catalysts, similarly, the diameter of the filaments also varied from 10 to 30 nm (Figure 3d,e). Nano-filament carbon with narrow hollow tube could be formed on both catalysts, Ni/Al_2O_3 and $La\text{-}Ni/Al_2O_3$ (Figure 3c,f respectively).

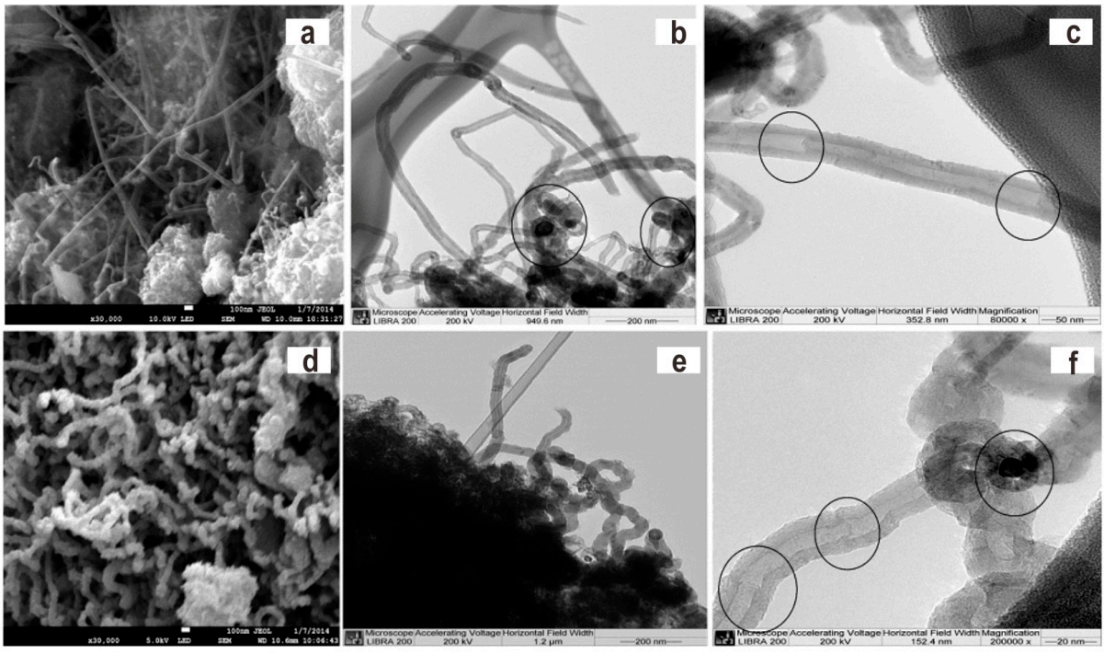

Figure 3. Field emission scanning electron microscopy (FE-SEM) and TEM images of deposited carbon on (**a**–**c**) Ni/Al_2O_3 and (**d**–**f**) $La\text{-}Ni/Al_2O_3$ catalysts after 72 h reaction (reprinted with permission from Ref. [55], copyright 2015 Elsevier).

3. Hydrocarbon Thermal Decomposition

Generally, carbon nanotubes can be formed as by-products of hydrocarbon catalytic decomposition processes. Recently, a new route adopting benzene decomposition over Ni nanoparticles under Argon atmosphere was described for the controllable synthesis of carbon nanorods (CNRs) and CNTs [45]. Moreover, it was found that, when using acetylene decomposition over Fe nanoparticles to synthesize CNTs, the addition of different amounts of H_2 led to the formation of CNTs with various helicities [46]. Afterwards, the same authors synthesized Fe/SnO_2 nanoparticles by using a combined sol-gel/reduction method and then used this catalyst in the pyrolysis of acetylene for selective synthesis of carbon nanofibers (CNFs), bamboo-like carbon nanotubes (CNTs), and chains of carbon nanospheres (CNSs) [47]. They found that the pyrolysis temperature, 500, 600, or 700 °C, had a considerable effect on the yield, morphology, and microwave absorption properties of the obtained materials.

A Fe-Ni nanoparticle catalyst supported on Mg(Al)O with a Fe/Ni atomic ratio of 65/35 was prepared by a novel nanoparticle synthesis and impregnation method. The catalyst was used in the non-oxidative dehydrogenation of methane for production of CO- and CO_2-free H_2 and carbon nanotubes (CNT) in the form of multi-walled nanotubes (MWNT) of relatively uniform diameter [48].

Mössbauer and X-ray absorption fine structure (XAFS) spectroscopic characterization carried out over the Fe-Ni np/Mg(Al)O catalyst suggested that during reaction with methane at 600–650 °C, an fcc Fe-Ni-C alloy of the invar type is formed that is active for dehydrogenation and formation of CNT. Moreover, TEM studies indicated that each nanoparticle was an active site for CNT growth in a tip growth mode. The resulting CNT generated were in the form of narrow sized bamboo-structured multi-walled nanotubes (B-MWNT) reflecting the tight size distribution of the Fe-Ni particles [48].

The structure of the carbon species can be affected by many factors, among them, the temperature has the most significant influence over others. Carbon nanotubes with a bamboo-shaped structure can be produced at a temperature higher than 727 °C [49]. The tri-metallic catalyst Ni-Co-Fe was used to synthesize bamboo-like multi-walled carbon nanotubes by methane decomposition at 1000 °C. The structure of multi-walled and bamboo-like carbon nanotubes with a diameter of 20 nm was observed through TEM [50]. Bamboo-like carbon nanotubes were successfully produced by Li et al. through direct catalytic chemical vapor deposition (CCVD) of methane over MgO-supported Cu/Mo catalysts [51].

Keane et al. [52] found that Ni/SiO_2 in the presence of H_2 promoted the growth of structured carbon from C_2H_4, C_2H_6, $C_2H_2Cl_2$, C_2HCl_3, $C_2H_4Cl_2$, and $C_2H_3Cl_3$. An effect of the reaction temperature and hydrocarbon type was found. The presence of the chloro group enhanced the carbon deposition with respect to ethane and ethane. Carbon fibers were generated from $C_2H_4Cl_2$, $C_2H_3Cl_3$, and $C_2H_2Cl_2$ and exhibited a "segmented" or "bamboo-shaped" structure with diameters ranging from 20 to 560 nm. On the contrary, catalytic decomposition of C_2HCl_3 produced predominantly nanospheres with a diameter of 35–680 nm, while nanofibers were produced from C_2H_4 and C_2H_6.

High carbon nanotube (CNT) yield was reported by Inoue et al. through decomposition of methane at temperatures below 680 °C over a spherical alumina Ni (10 wt %) supported catalyst [53]. When increasing the temperature, to values >700 °C, however, the carbon formation rate decreased. TEM observation revealed that the structure of CNTs was identical independently of the range of temperature, suggesting the irrelevance between temperature and structure. However, the decrease of solubility of carbon in the nickel particles at higher temperature resulted in longer compartment size and a less bamboo-like structure.

González et al. [57] prepared bamboo-like CNTs by two kinds of Ni catalyzed methane thermal decompositions that were carried out in a thermogravimetric analyzer. A bamboo-like structure was observed by TEM analysis and the images are shown in Figure 4.

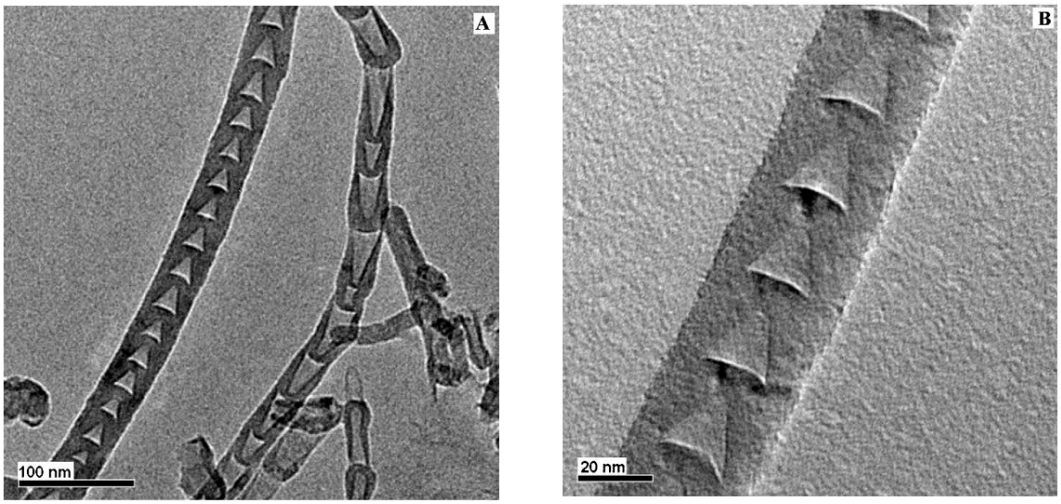

Figure 4. Bamboo-like carbon nanotubes (CNTs) obtained by methane thermal decomposition with different catalysts (**A**) Ni-Tween 20 and (**B**) Ni-$NaBH_4$ nanoparticles (reprinted with permission from Ref. [57], copyright 2011 Elsevier).

The internal tubes of CNTs were filled by well-defined conical holes (Figure 4B), whose diameter was around 20 nm. The resulting carbon nanotubes with average external diameter between 30 and 60 nm (shown in Figure 4A) which were much larger than that of the original nickel nanoparticles (3–12 nm) suggested that agglomeration of Ni to form larger nanoparticles happened during the CNTs growth process. Formation of larger Ni nanoparticles induced the growth of the bamboo-like CNTs.

The schematic illustration of the growth process of bamboo-like CNTs over Ni nanoparticles catalyst is depicted in Figure 5 [57]. Carbon formation occurs over the surface of the Ni particle during the methane thermal decomposition process, after that, a diffusion step over the droplet shaped metal particles takes place. Stress force generated during the formation process of the carbon shells pushes the Ni particles toward the growing direction, which results in a jump of the Ni particle followed by the formation of conical holes. The bamboo-like structure of the carbon nanotubes was produced when the above process occurred repeatedly.

Carbon filaments and nano-sized carbon particles as well as bamboo-like carbon nanotubes were fabricated from methane decomposition on the Ni-Cu/Al_2O_3 catalyst at 720–830 °C by Li et al. [58]. The morphology of the final product was influenced by several factors such as the Cu doping content into the catalyst, the constituent of the feed gas, and the reaction temperature. Metal nanoparticles which exhibited quasi-liquid state had a significant effect in the formation of bamboo-shaped CNTs during the growth process of the carbon.

Pure bamboo-like CNTs were obtained with a gas composition of CH_4/H_2 (1:2 H_2) on Ni-Cu/Al_2O_3 nanoparticles at 720–770 °C. Compared with pure Ni/Al_2O_3 catalyst, the doping of Cu into Ni/Al_2O_3 catalyst resulted in the formation of bamboo-like carbon nanotubes from methane. The shape of the metal particle had a strong effect on the structure and morphology of the formed carbon. Among the different shapes of the metal particles, the quasi-liquid state metal particle was related to the formation of bamboo-like CNTs. The existence of quasi-liquid state metal particles in the reaction system was attributed to the correct addition content of the copper, the high ratio of hydrogen in the gas feed, and the growth process of the carbon. In the carbon shells growing process, the capillary force generated at the interface of metal particle–carbon shell accumulated, then the capillary force worked as the driving force for the jump of the quasi-liquid state metal particle to form the bamboo-like CNTs. Pressure generated from the evaporation of metal inside the hollow and the release of hydrogen from the newly formed carbon sheets at the back part of the metal together accumulated to give an internal stress force for the smooth forward movement of metal particles.

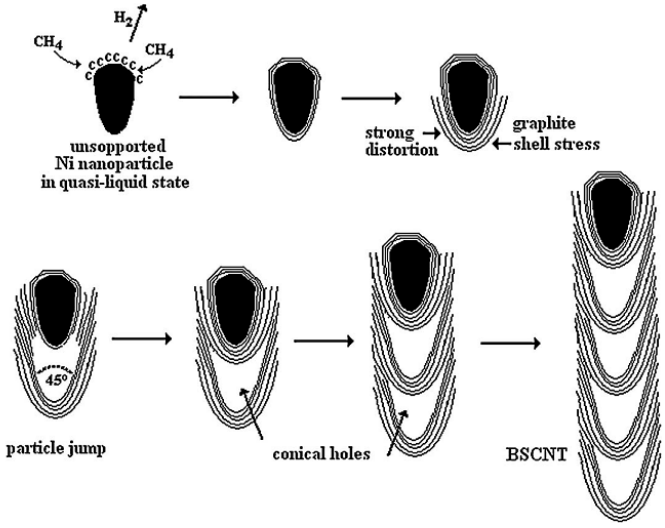

Figure 5. Formation mechanism of bamboo-like carbon nanotubes (reprinted with permission from Ref. [57], copyright 2011 Elsevier).

Carbon nanotubes were synthesized by the decomposition of methane over Ni and Ni-Cu alloy as catalysts (Figure 6) [59]. The result revealed that the introduction of copper had a significant influence on the formation of the product, both improvement of methane conversions and carbon yields were observed. Moreover, not only the catalyst composition but also the reaction temperature would have resulted in the various morphologies of carbon materials, herringbone carbon nanofibers, platelet CNFs, bamboo-like CNFs, branched CNFs, multi-branched CNFs, and onion-like carbons being obtained.

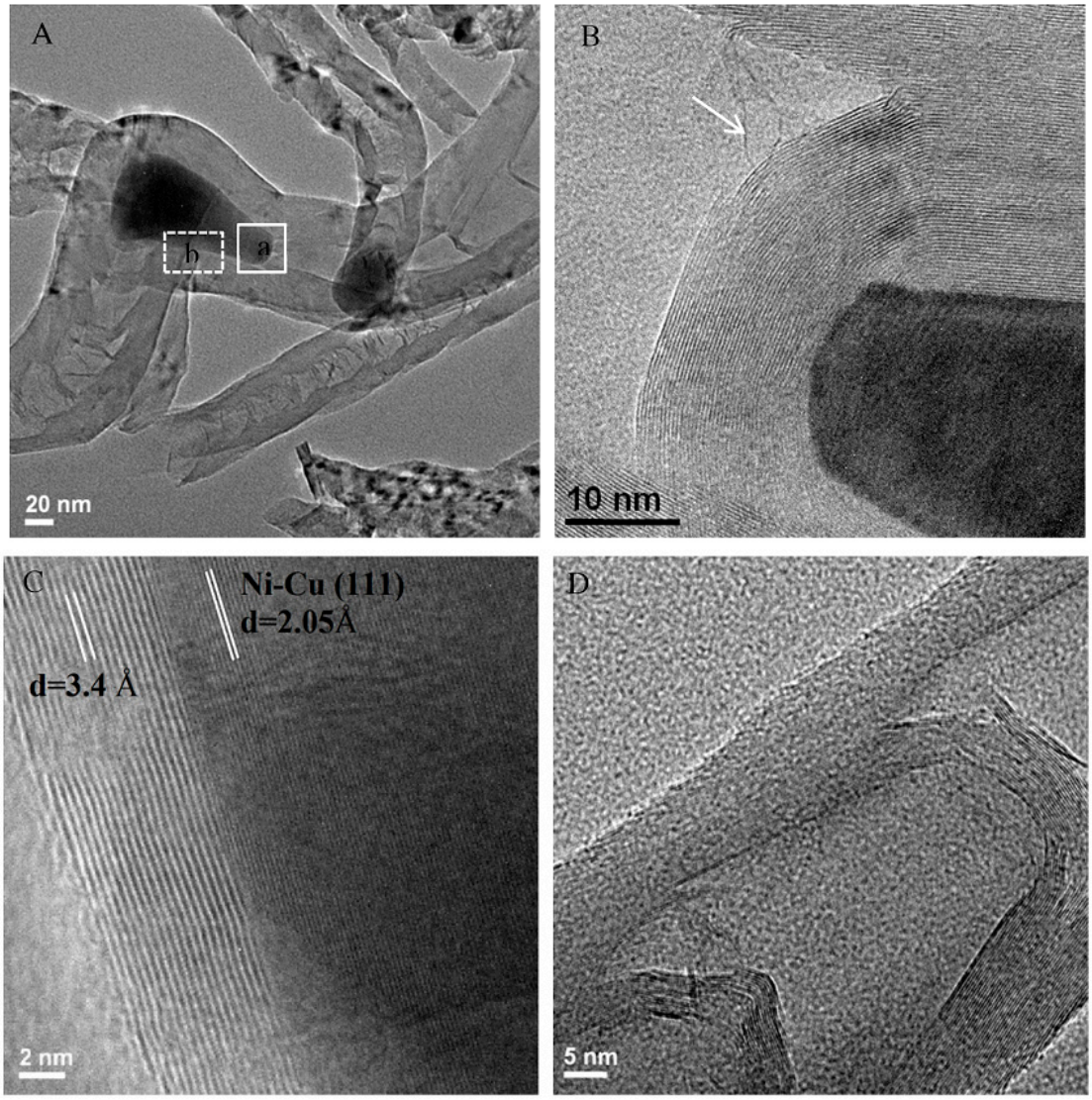

Figure 6. TEM images of the bamboo-like carbon nanofibers (CNFs) on the $Ni_{47}Cu_{53}$/CNT catalyst (**A**) bamboo-like CNFs, (**B**) magnification of the region marked "a" in (**A**,**C**) magnification of the region marked "b" in (**A**,**D**) a typical bamboo-like CNF (reprinted with permission from Ref. [59], copyright 2015 Elsevier).

Typical bamboo-like CNFs obtained from the $Ni_{47}Cu_{53}$/CNT catalyst at 750 °C are shown in Figure 6.

An overview of the bamboo-shaped CNFs and typical bamboo-shaped CNF is reported in Figure 6A,D respectively. To have a better understanding of the formation of bamboo-shaped CNFs, the magnification images of the marked "a" and "b" in Figure 6A were presented in Figure 6B,C respectively. The lattice fringe which represented Ni-Cu (111) with a d-spacing of 0.21 nm was parallel

but smaller to the graphitic (002) lattice fringe which was 0.34 nm (shown in Figure 6C). Uniformly-size hollow compartments structure which the bamboo-like CNFs possessed were separated by transversely extended graphene layers. The elongated conical shaped Ni-Cu alloy particle was closely surrounded by graphitic layers as shown in Figure 6B. It should be noted that the high Cu content in the Ni-Cu based catalysts and higher temperatures (>700 °C) were exclusive to the formation of bamboo-like CNFs. The introduction of lower melting point Cu into the catalyst led to the formation of quasi-liquid state of Ni-Cu alloy particles at the reaction temperatures.

4. Special Chemical Vapor Deposition

Due to the potential applications of CNTs, inexpensive and scalable growth techniques need to be achieved for the synthesis of such materials. Chemical vapor deposition (CVD) with the aid of transition metal catalysts has been proven as a feasible technique since pure and control size CNTs have been successfully synthesized on different pattern substrates by this method. Properties of the final carbon product such as the diameter of the tubes and the microstructure, i.e., the shape are related to the following factors: the type of metal nanoparticle catalysts as well as the precursor and processing conditions. Numerous raw materials such as hydrocarbons (CH_4, C_2H_2, C_2H_4, etc.) or CO feedstocks and various metal particle catalysts such as Fe, Ni, or Co have been used for the growth of MWCNT on different substrates by CVD.

Carbonaceous material with entangled tubular arrangements was prepared by the catalytic chemical vapor deposition (CCVD) method by Santamaria et al. [60]. In the CCVD process a glycerol-ethanol mixture was used as carbon source and $LaNiO_3$ perovskite as catalyst, the structure of carbonaceous material corresponded to MWCNTs whose morphology features were determined by the reaction temperature (Figure 7). Standard MWCNTs with parallel graphene layers were obtained at 700 °C, whereas bamboo-like MWCNT morphology was prepared at higher temperature (i.e., 800 °C and 900 °C), meanwhile an increase in outer diameter of the MWCNT with the increment of reaction temperature was also observed. The relationship between the morphology of the synthesized CNTs by the catalytic chemical vapor deposition method, in which an ethanol-glycerol mixture was used as carbon source, and different reaction temperatures was further investigated by the author.

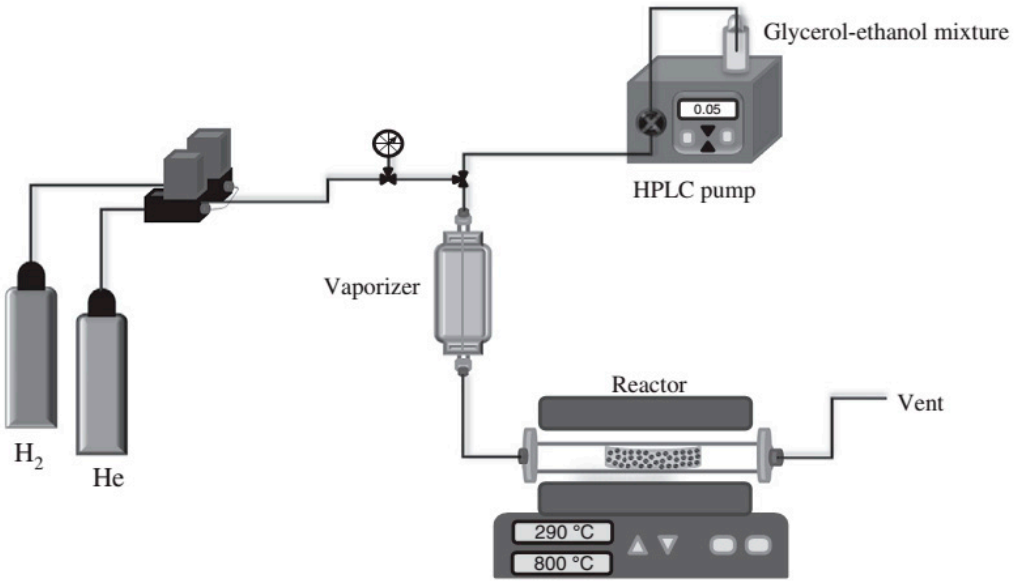

Figure 7. Sketch map of the chemical vapor deposition (CVD) (reprinted with permission from Ref. [60], copyright 2014 Elsevier).

CNTs were prepared through detonation-assisted CVD by Wang et al. [61]. Detonation of explosives on a micro-second time scale provided the energy for the fabrication of carbon species to

nanotubes. Intermediate objects surviving within the detonation process provided the possibility to trace the formation of CNTs. Detonation-assisted CVD was carried out in a 10 mL sealed stainless steel pressure vessel which was connected to a pressure gauge. Reaction was induced by an external heating process (20 °C/min) to 310 °C. Pressure rose to 40 MPa (shock wave) and temperature increased to 900 °C when the detonation occurred inside the vessel. After the vessel was cooled in air and the gaseous products were emptied, solid products were obtained.

Typical bamboo-like CNTs were fabricated and the TEM images are shown in Figure 8a,b. Due to the different distribution of bamboo knots, the structure of bamboo-like CNTs was divided into compartments with different dimensions and shapes. Formation of the compartments in bamboo tubes resulted from the metal particle catalyst moving along the growth direction. Therefore, the production of the CNTs with the unique structure of compartments and bamboo knots demonstrated that the metal particle catalyst underwent a repetitive process of elongation and contraction during the CNT growth. The step between the outer wall and the knot observed from the HRTEM image in Figure 8c revealed that the outermost graphene sheets grow continuously along the tube axis direction. Figure 8d illustrates the structure model of the bamboo knot. The formation mechanism of bamboo knot involves the nucleation and growth of the bamboo knot occurring on the multistep Ni-graphite edges, instead of precipitating on the top surface of the metal particle. Figure 8e shows the metal particle that started to contract but was wrapped by the graphene layer, displaying the tip-growth model during the formation of CNTs. During the growth process, the fluctuation of the metal particle catalyst resulted in the appearance of a compartment between its asymmetric growth orientation and the bamboo knot. The nucleation process of the bamboo knot was observed, as shown in Figure 8f,g. The result in that graphene sheets (bamboo knot) were formed at a stepped Ni surface is in agreement with the above interpretation. Thus, the tube growth was caused by the repetitive elongation and contraction process of the metal particle catalyst, meanwhile the nucleation of graphene sheets occurred on the edges of multistep Ni-graphite.

Vertically aligned MWCNTs were synthesized through microwave plasma enhanced chemical vapor deposition (MPECVD) by Brown et al. [62]. A mixed gas of ammonia/methane was used as the carbon source and the reaction was carried out on thermally oxidized silicon substrates with a platinum thin film catalyst. TEM images of the Pt-CNT samples are presented in Figure 9a,b. The bamboo-like structure which contained a series of hollow and periodic compartments and bamboo knots was observed by TEM images. Compared with nanotubes where the metal particles were encapsulated in the tips, the carbon nanotubes whose tips were void of metal particles tended to be shorter in length. A high density of metal particles, left behind after the removal of nanotubes-epoxy specimen for TEM preparation, was observed embedded in the detached substrate as shown in Figure 9c,d. Base-growth mode was proved by the above observations as shown in Figure 9.

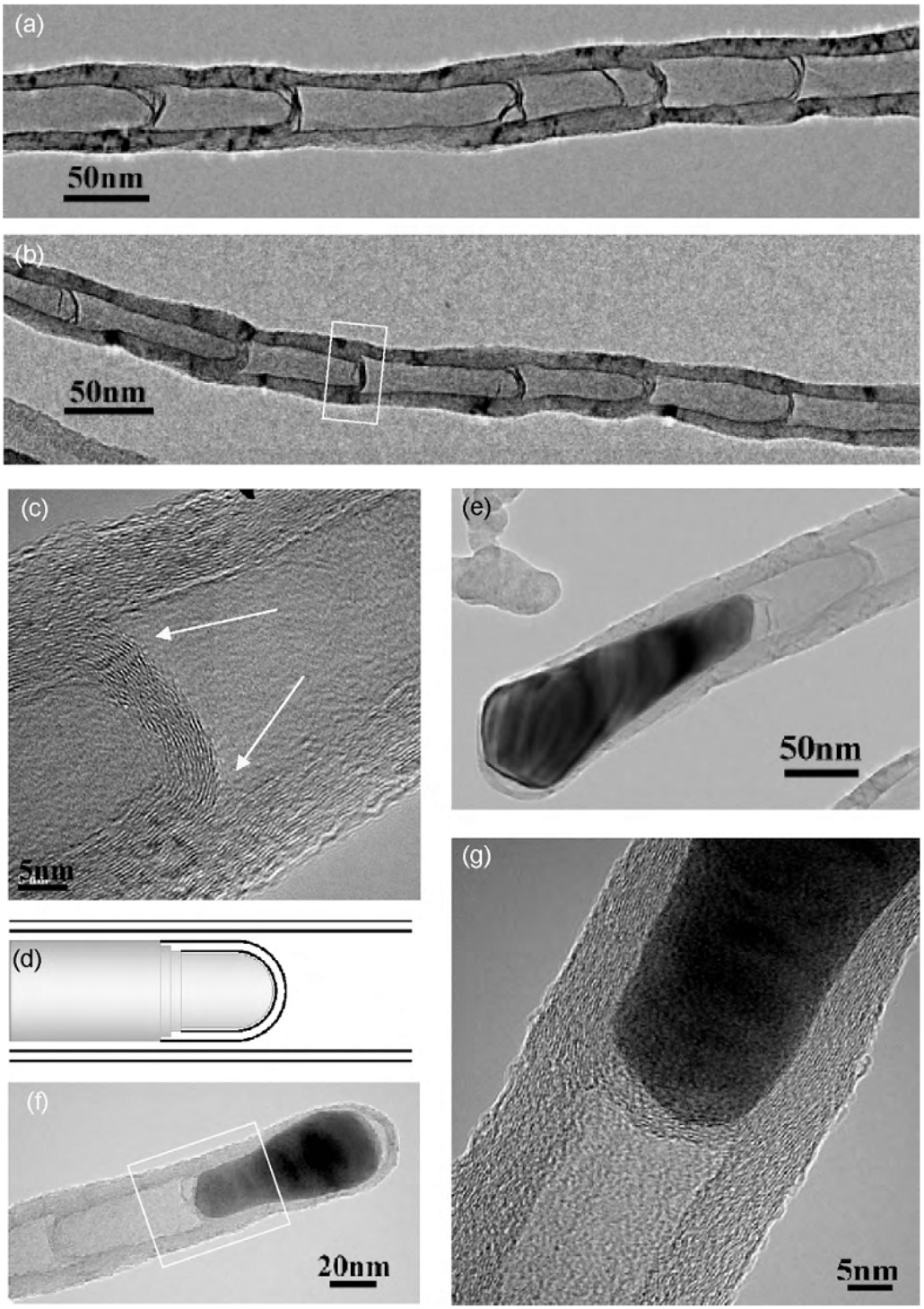

Figure 8. (**a**,**b**) TEM images of bamboo-like CNTs; (**c**) HRTEM image and (**d**) physical model of the bamboo knot; (**e**) TEM image of a reacting catalyst particle; and (**f**,**g**) TEM and HRTEM images of a forming bamboo knot (reprinted with permission from Ref. [61], copyright 2010 Elsevier).

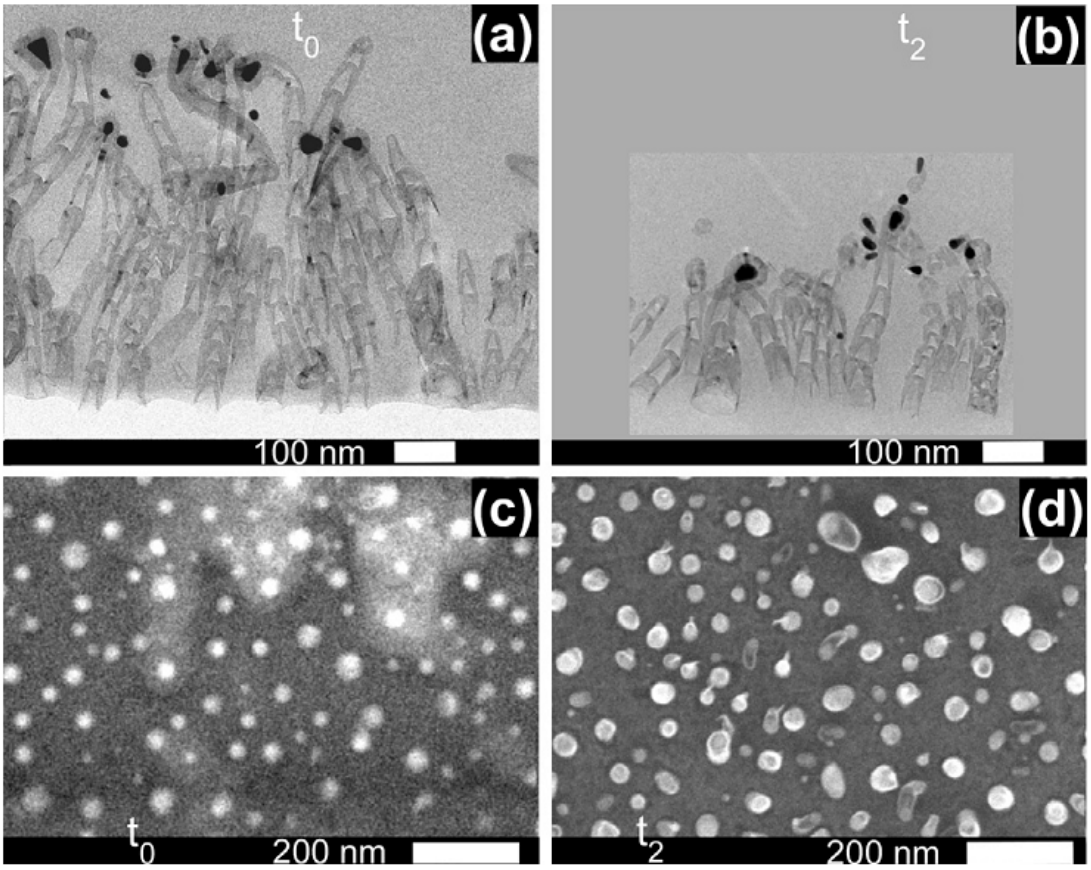

Figure 9. TEM images of Pt-CNT after a pretreatment of (**a**) 0 and (**b**) 3 min; Corresponding SEM images (**c**,**d**); respectively (reprinted with permission from Ref. [62], copyright 2011 Elsevier).

5. Pyrolysis and Gasification from Plastic Wastes

Numerous researches dealing with hydrogen production by pyrolysis and gasification of waste plastic have been reported recently [63–69]. To improve the efficiency of the hydrogen production process, the effect of many catalysts has been investigated. Compared with the so far discussed CVD method for CNTs production, gasification of waste plastics for the fabrication of CNTs has received less attention, although such a method is worthy of review being a cheap carbon source. By adjusting the reaction conditions and the nature of catalysts used for the plastic gasification reaction, both CNTs and hydrogen can be obtained in the presence of steam. Few investigations on the simultaneous synthesis of hydrogen and carbon nanotubes from waste plastic using thermo-chemical methods have been described. The influence of metal addition to Ni-based catalysts on the production of hydrogen and CNTs from waste plastic was investigated by Williams et al. [70]. The catalysts were prepared by co-precipitation and waste polypropylene was chosen as the representative of waste plastic. In their study, the activity of different types of Ni-based ternary mixed oxide catalysts, Ni-M-Al (M = Zn, Mg, Ca, Ce or Mn) was investigated by adopting catalytic steam reforming of waste plastic polypropylene. The use of catalysts prepared by a co-precipitation method for hydrogen and CNT production was carried out in a two stage fixed bed reactor (Figure 10). The influence of the metal content added to the Ni-based catalysts and the effect of the water injection rate during the reaction were studied. Bamboo-like carbon nanotubes and multi-walled carbon nanotubes with parallel graphene layers were detected by TEM over Ni-Mn-Al catalyst [70]. Afterwards, the same group, Williams et al. [71], investigated nickel, iron, cobalt, and copper catalysts, prepared by an impregnation method, to produce carbon nanotubes and hydrogen gas from an LDPE feedstock.

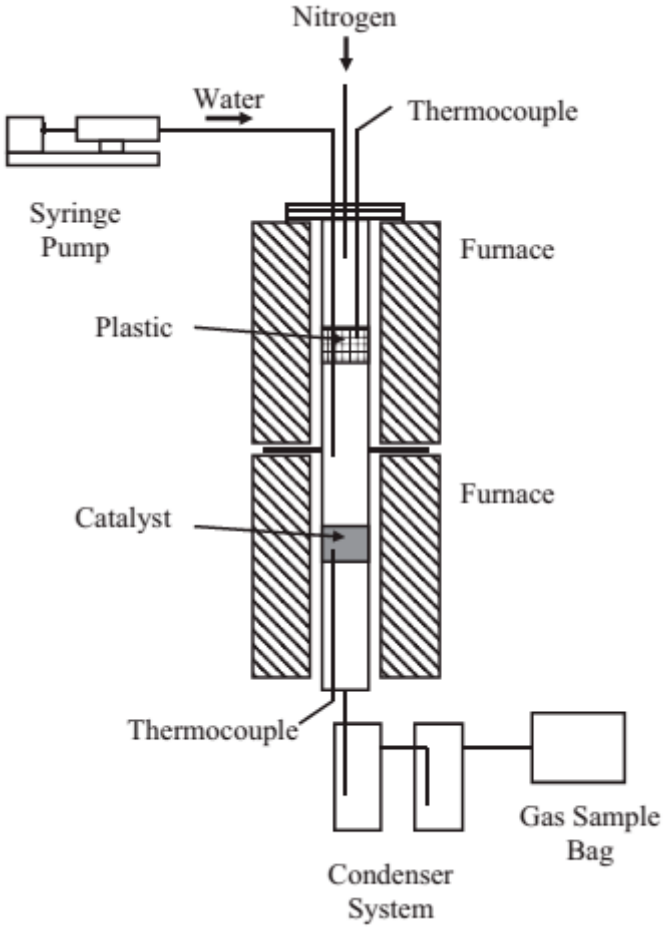

Figure 10. Sketch map of the reforming installation (reprinted with permission from Ref. [70], copyright 2015 Elsevier).

To obtain large yields of both products, carbon nanotubes, and hydrogen, a two-stage catalytic pyrolysis process was proposed. Bamboo-like carbon nanotubes were also observed. Before the evolved gases passed to a second stage, plastics samples were pyrolysed in nitrogen at 600 °C and carbon deposition onto the catalysts was obtained when the temperature was increased to 800 °C.

Formation of carbon nanotubes with a filament structure takes place over Ni as observed by TEM investigation, as shown in Figure 11a. The diameters of carbon nanotubes varied between 15 and 30 nm and lengths ranged up to some micrometers. Carbon nanotubes and bamboo-like nanotubes as well as the existence of a number of loose metal particles in the catalyst were observed by TEM images. The presence of metal particles inside the carbon nanotubes suggested that tip, instead of base growth mechanism, occurs.

Multi-walled carbon nanotubes and bamboo-like structure carbon nanotubes were also obtained using iron catalyst, as shown in Figure 11b. Compared with the nickel catalyst, CNTs with a larger diameter were produced. The presence of Fe metal particles larger than those of Ni catalyst resulted in the formation of larger diameter bamboo-like CNTs.

Multi-walled carbon nanotubes with a much narrower diameter were fabricated by a cobalt based catalyst (see Figure 11c). Only very few loose metal particles were found in the TEM images. The diameters of carbon nanotubes ranged from 5–20 nm and the lengths of the carbon nanotubes were up to a number of micrometers. The strong interaction between cobalt and the support, as deduced by temperature-programmed reduction (TPR) results, prevented sintering of the metal particles, therefore, favoring formation of smaller CNT diameters. Moreover, it cannot be excluded that a very strong

metal support interaction may inhibit production of CNTs because cobalt metal particles are too small for CNTs growth or too strongly attached to the support.

Only amorphous carbon was formed over the copper based catalyst, contrary to other metals. TEM images revealed the presence of very large Cu particles that are likely too large to grow carbon nanotubes on the surface. According to TPR curves, CuO particles formed on the calcined sample were easily reduced leading to significant sintering.

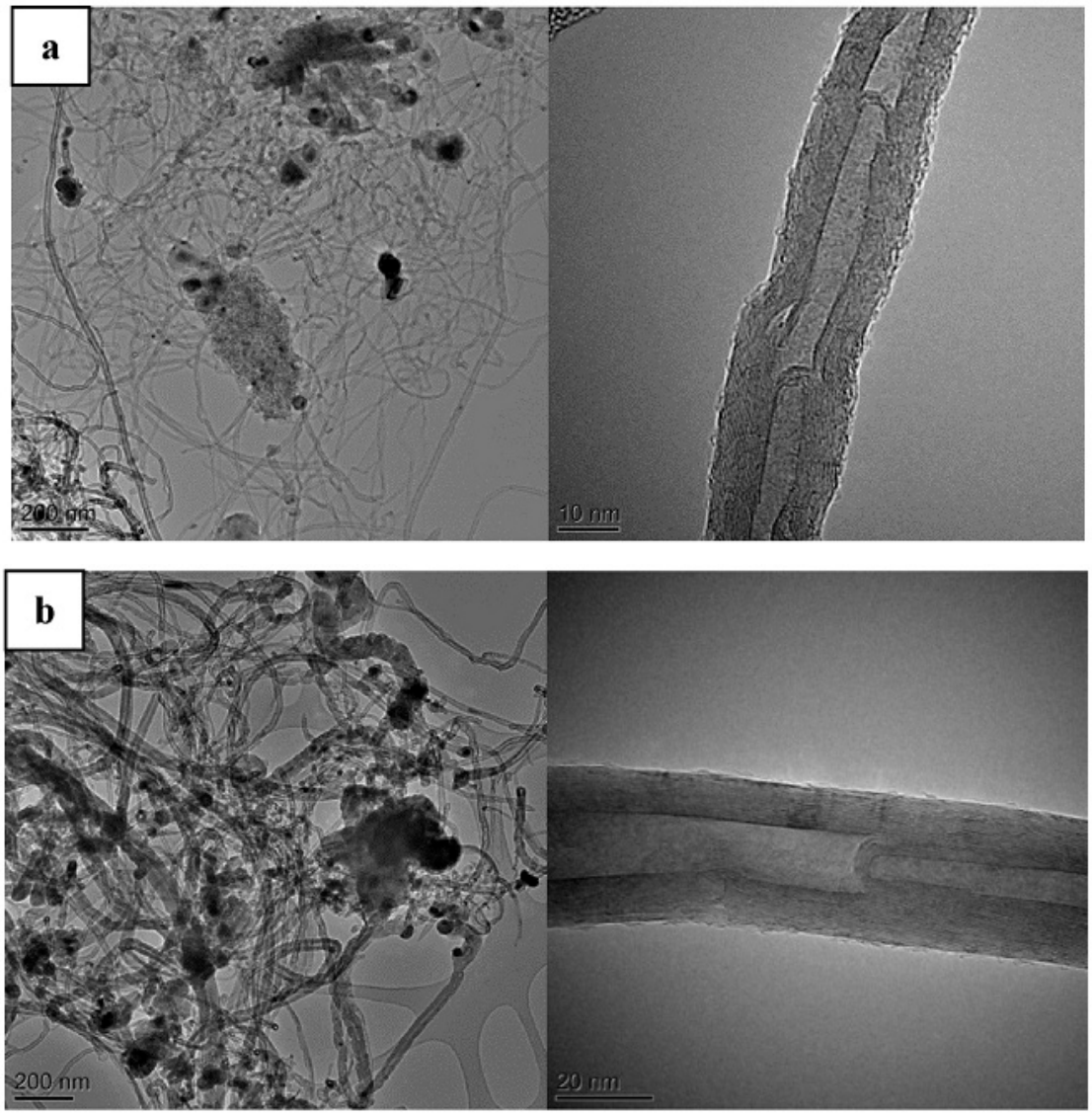

Figure 11. *Cont.*

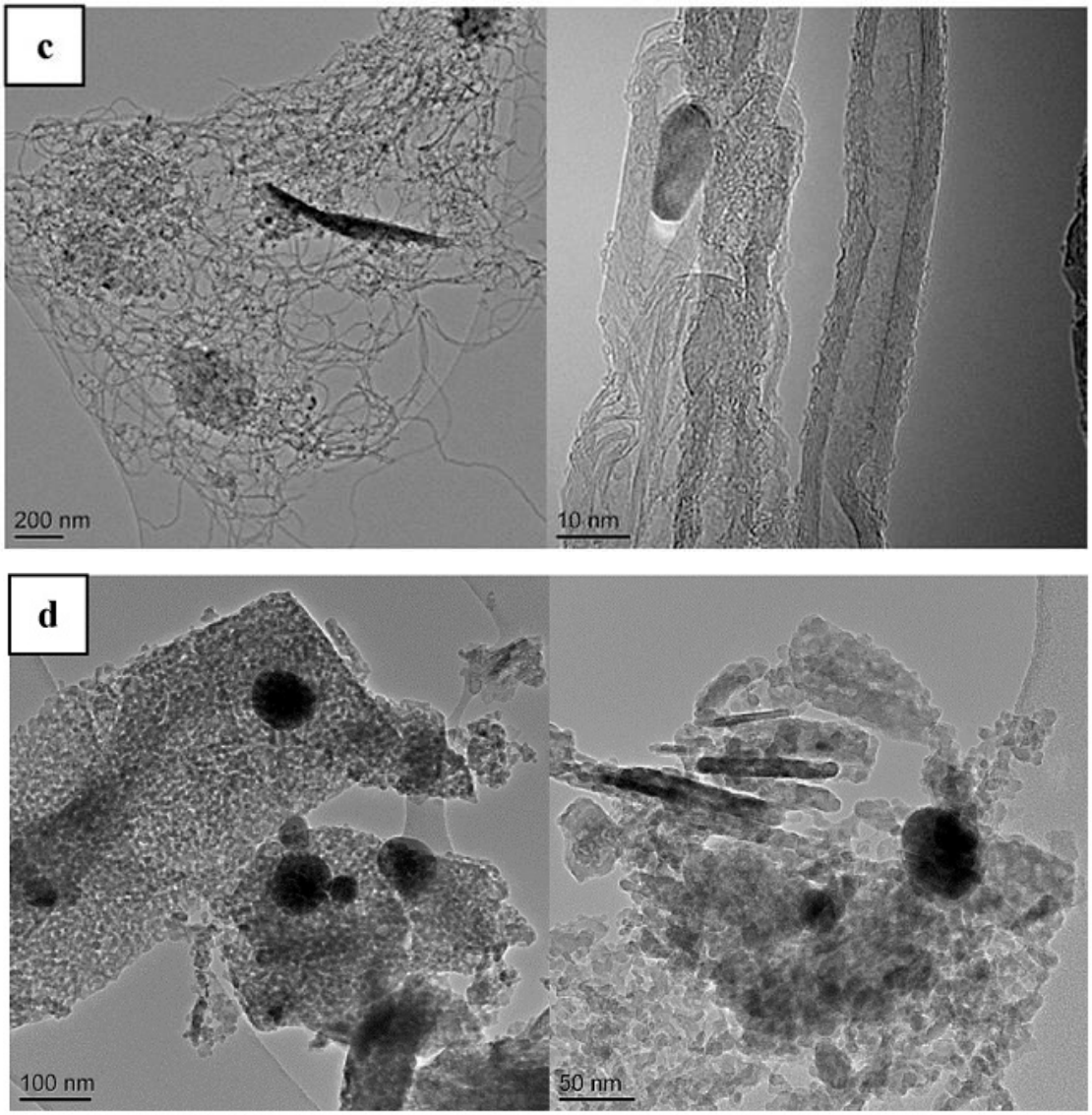

Figure 11. TEM images of the used Al_2O_3 catalysts doped by different metals: (**a**) Ni; (**b**) Fe; (**c**) Co and (**d**) Cu (reprinted with permission from Ref. [71], copyright 2016 Elsevier).

6. Conclusions

This review depicts some preparation methods for bamboo-like carbon nanotubes. The most commonly employed are dry reforming reactions, hydrocarbon thermal decomposition, and special chemical vapor deposition. Among other methods, pyrolysis and gasification of plastic wastes are particular examples.

Although the dry reforming reaction is not the most used method for large-scale production of bamboo-like carbon nanotubes at a relatively low cost, it can produce both high quality hydrogen and bamboo-like carbon nanotubes at relatively low temperature. Despite the high yield of bamboo-like carbon nanotubes and the simple preparation process, the products obtained from the hydrocarbon thermal decomposition and special chemical vapor deposition methods suffer from relatively low purity and unsatisfactory structure. Besides, the reaction temperature and the catalysts type may also affect the nature of products. As for the pyrolysis and gasification of waste plastic, this method takes advantage of using waste plastic as the carbon source as well as hydrogen. Similar to the former methods, the final product is also influenced by the reaction temperature, the catalyst composition as

well as by the waste plastic types. Based on microscopic characterizations, it appears clear that there is a strong correlation between the catalytic activity and the typology/amount of carbonaceous deposits. The best catalysts are those with the best combination of these two parameters (high amount of carbon nanotubes together with low quantity of total carbon).

Moreover, in this review it has been highlighted that the key factor for the formation of bamboo shaped carbon nanotubes is the presence of the quasi-liquid state of the metal nanoparticles during the carbon growth process. Therefore, for improved catalytic activity and stability of the dry reforming catalysts by means of the formation of bamboo-like carbon nanotubes, we should design and prepare deformable metal nanoparticles during the growth of the carbon.

Furthermore, we expect that further progress in the production of bamboo-like carbon nanotubes over dry reforming catalysts can be achieved by the following:

1. Density functional theory studies of the interaction between dry reforming catalysts and bamboo-like carbon nanotubes will lead to the design and preparation of novel catalysts;
2. The comprehensive understanding of the formation mechanisms of bamboo-like carbon nanotubes and their effects on catalytic performance will lead to the design and preparation of other catalysts.

Acknowledgments: Financial support was provided by National Natural Science Foundation of China (Nos. 50771082 and 60776822). The Project Supported by Natural Science Basic Research Plan in Shaanxi Province of China (Program No. 2017JQ5116).

Author Contributions: K.K., M.Q. and F.P. analyzed the literature and selected proper references; Z.J., H.W. and L.F.L. critically discussed the data and wrote the paper.

Conflicts of Interest: The authors declare no conflict of interest.

References

1. Zhang, P.; Qiao, Z.A.; Dai, S. Recent advances in carbon nanospheres: Synthetic routes and applications. *Chem. Commun.* **2015**, *51*, 9246–9256. [CrossRef] [PubMed]
2. Zhang, B.; Kang, F.; Tarascon, J.M.; Kim, J.K. Recent advances in electrospun carbon nanofibers and their application in electrochemical energy storage. *Prog. Mater. Sci.* **2016**, *76*, 319–380. [CrossRef]
3. Jia, X.; Wei, F. Advances in production and applications of carbon nanotubes. *Top. Curr. Chem.* **2017**, *375*, 18. [CrossRef] [PubMed]
4. Xu, H.; Yin, X.; Zhu, M.; Han, M.; Hou, Z.; Li, X.; Zhang, L.; Cheng, L. Carbon hollow microspheres with a designable mesoporous shell for high-performance electromagnetic wave absorption. *ACS Appl. Mater. Interfaces* **2017**, *9*, 6332–6341. [CrossRef] [PubMed]
5. Lv, H.; Yang, Z.; Cheng, Y.; Wang, L.; Zhang, B.; Zhao, Y.; Xu, Z.; Ji, G. A brief introduction to the fabrication and synthesis of graphene based composites for the realization of electromagnetic absorbing materials. *J. Mater. Chem. C* **2017**, *5*, 491–512. [CrossRef]
6. Lv, H.; Guo, Y.; Wu, G.; Ji, G.; Zhao, Y.; Xu, Z. Interface polarization strategy to solve electromagnetic wave interference issue. *ACS Appl. Mater. Interfaces* **2017**, *9*, 5660–5668. [CrossRef] [PubMed]
7. Lv, H.; Zhang, H.; Ji, G.; Xu, Z. An interface strategy to achieve tunable high frequency attenuation. *ACS Appl. Mater. Interfaces* **2016**, *8*, 6529–6538. [CrossRef] [PubMed]
8. Zha, J.W.; Huang, N.; He, K.Q.; Dang, Z.M.; Shi, C.Y.; Li, R.K.Y. Electrospun poly(ethylene oxide) nanofibrous composites with enhanced ionic conductivity as flexible solid polymer electrolytes. *High Volt.* **2017**, *2*, 25–31. [CrossRef]
9. Wan, L.; Zhang, X.; Wu, G.; Feng, A. Thermal conductivity and dielectric properties of bismaleimide-cyanate ester copolymer. *High Volt.* **2017**. [CrossRef]
10. Qing, Y.; Wen, Q.; Luo, F.; Zhou, W.; Zhu, D. Graphene nanosheets/$BaTiO_3$ ceramics as highly efficient electromagnetic interference shielding materials in the X-band. *J. Mater. Chem. C* **2016**, *4*, 371–375.
11. Wu, G.; Wu, H.; Wang, K.; Zheng, C.; Wang, Y.; Feng, A. Facile synthesis and application of multi-shelled SnO_2 hollow spheres in lithium ion battery. *RSC Adv.* **2016**, *6*, 58069–58076. [CrossRef]

12. Liotta, L.F.; Wu, H.; Pantaleo, G.; Venezia, A.M. Co_3O_4 nanocrystals and Co_3O_4–MO_x binary oxides for CO, CH_4 and VOC oxidation at low temperatures: A review. *Catal. Sci. Technol.* **2013**, *3*, 3085–3102. [CrossRef]
13. Wu, H.; Wang, L.; Zhang, J.; Shen, Z.; Zhao, J. Catalytic oxidation of benzene, toluene and p-xylene over colloidal gold supported on zinc oxide catalyst. *Catal. Commun.* **2011**, *12*, 859–865. [CrossRef]
14. Wu, H.; Wang, L.; Wang, Y.; Guo, S.; Shen, Z. Enhanced microwave performance of highly ordered mesoporous carbon coated by Ni_2O_3 nanoparticles. *J. Alloys Compd.* **2012**, *525*, 82–86. [CrossRef]
15. Wu, H.; Wu, G.; Ren, Y.; Yang, L.; Wang, L.; Li, X. Co^{2+}/Co^{3+} ratio dependence of electromagnetic wave absorption in hierarchical $NiCo_2O_4$–$CoNiO_2$ hybrids. *J. Mater. Chem. C* **2015**, *3*, 7677–7690. [CrossRef]
16. Wu, H.; La Parola, V.; Pantaleo, G.; Puleo, F.; Venezia, A.M.; Liotta, L.F. Ni-based catalysts for low temperature methane steam reforming: Recent results on Ni-Au and comparison with other bi-metallic systems. *Catalysts* **2013**, *3*, 563–583. [CrossRef]
17. Wu, H.; Wu, G.; Wang, L. Peculiar porous α-Fe_2O_3, γ-Fe_2O_3 and Fe_3O_4nanospheres: Facile synthesis and electromagnetic properties. *Powder Technol.* **2015**, *269*, 443–451. [CrossRef]
18. Wu, H.; Pantaleo, G.; La Parola, V.; Venezia, A.M.; Collard, X.; Aprile, C.; Liotta, L.F. Bi-and trimetallic Ni catalysts over Al_2O_3 and Al_2O_3-MO_x (M = Ce or Mg) oxides for methane dry reforming: Au and Pt additive effects. *Appl. Catal. B* **2014**, *156*, 350–361. [CrossRef]
19. Wu, H.; Wang, L.; Shen, Z.; Zhao, J. Catalytic oxidation of toluene and *p*-xylene using gold supported on Co_3O_4 catalyst prepared by colloidal precipitation method. *J. Mol. Catal. A* **2011**, *351*, 188–195. [CrossRef]
20. Wu, H.; Wang, L. Shape effect of microstructured CeO_2 with various morphologies on CO catalytic oxidation. *Catal. Commun.* **2011**, *12*, 1374–1379. [CrossRef]
21. Wu, H.; Pantaleo, G.; Di Carlo, G.; Guo, S.; Marcì, G.; Concepción, P.; Venezia, A.M.; Liotta, L.F. Co_3O_4 particles grown over nanocrystallineCeO_2: Influence of precipitation agents and calcination temperature on the catalytic activity for methane oxidation. *Catal. Sci. Technol.* **2015**, *5*, 1888–1901. [CrossRef]
22. Wu, H.; Pantaleo, G.; Venezia, A.M.; Liotta, L.F. Mesoporous silica based gold catalysts: Novel synthesis and application in catalytic oxidation of CO and volatile organic compounds (VOCs). *Catalysts* **2013**, *3*, 774–793. [CrossRef]
23. Wu, G.; Cheng, Y.; Ren, Y.; Wang, Y.; Wang, Z.; Wu, H. Synthesis and characterization of γ-Fe_2O_3@C nanorod-carbon sphere composite and its application as microwave absorbing material. *J. Alloys Compd.* **2015**, *652*, 346–350. [CrossRef]
24. Wu, G.; Cheng, Y.; Xie, Q.; Jia, Z.; Xiang, F.; Wu, H. Facile synthesis of urchin-like ZnO hollow spheres with enhanced electromagnetic wave absorption properties. *Mater. Lett.* **2015**, *144*, 157–160. [CrossRef]
25. Wu, G.; Cheng, Y.; Xiang, F.; Jia, Z.; Xie, Q.; Wu, G.; Wu, H. Morphology-controlled synthesis, characterization and microwave absorption properties of nanostructured 3D CeO_2. *Mater. Sci. Semicond. Process.* **2016**, *41*, 6–11. [CrossRef]
26. Wu, G.; Cheng, Y.; Wang, Z.; Wang, K.; Feng, A. In situ polymerization of modified graphene/polyimide composite with improved mechanical and thermal properties. *J. Mater. Sci. Mater. Electron.* **2017**, *28*, 576–581. [CrossRef]
27. Wu, G.; Li, J.; Wang, K.; Wang, Y.; Pan, C.; Feng, A. In situ synthesis and preparation of TiO_2/polyimide composite containing phenolphthalein functional group. *J. Mater. Sci. Mater. Electron.* **2017**, *28*, 6544–6551. [CrossRef]
28. Wu, G.; Cheng, Y.; Wang, K.; Wang, Y.; Feng, A. Fabrication and characterization of OMMt/BMI/CE composites with low dielectric properties and high thermal stability for electronic packaging. *J. Mater. Sci. Mater. Electron.* **2016**, *27*, 5592–5599. [CrossRef]
29. Wu, G.; Wang, Y.; Wang, K.; Feng, A. The effect of modified AlN on the thermal conductivity, mechanical and thermal properties of AlN/polystyrene composites. *RSC Adv.* **2016**, *6*, 102542–102548. [CrossRef]
30. Pan, C.; Kou, K.; Jia, Q.; Zhang, Y.; Wu, G.; Ji, T. Improved thermal conductivity and dielectric properties of hBN/PTFE composites via surface treatment by silane coupling agent. *Compos. Part B Eng.* **2017**, *111*, 83–90. [CrossRef]
31. Gu, J.; Dong, W.; Xu, S.; Tang, Y.; Ye, L.; Kong, J. Development of wave-transparent, light-weight composites combined with superior dielectric performance and desirable thermal stabilities. *Compos. Sci. Technol.* **2017**, *144*, 185–192. [CrossRef]

32. Gu, J.; Xu, S.; Zhuang, Q.; Tang, Y.; Kong, J. Hyperbranched polyborosilazane and boron nitride modified cyanate ester composite with low dielectric loss and desirable thermal conductivity. *IEEE Trans. Dielectr. Electr. Insul.* **2017**, *24*, 784–790. [CrossRef]
33. Iijima, S. Helical microtubules of graphitic carbon. *Nature* **1991**, *354*, 56–58. [CrossRef]
34. Wang, W.; Yang, K.Q.; Gaillard, J.; Bandaru, P.R.; Rao, A.M. Rational synthesis of helically coiled carbon nanowires and nanotubes through the use of tin and indium catalysts. *Adv. Mater.* **2008**, *20*, 179–182. [CrossRef]
35. Kang, Z.K.; Wang, E.B.; Mao, B.D.; Su, Z.M.; Gao, L.; Lian, S.Y.; Xu, L. Controllable fabrication of carbon nanotube and nanobelt with a polyoxometalate-assisted mild hydrothermal process. *J. Am. Chem. Soc.* **2005**, *127*, 6534–6535. [CrossRef] [PubMed]
36. Kleitz, F.; Choi, S.H.; Ryoo, R. Cubic *Ia3d* large mesoporous silica: Synthesis and replication to platinum nanowires, carbon nanorods and carbon nanotubes. *Chem. Commun.* **2003**, *17*, 2136–2137. [CrossRef]
37. Herring, A.M.; Mckinnon, J.T.; Mccloskey, B.D.; Filley, J.; Gneshin, K.W.; Pavelka, R.A. A novel method for the templated synthesis of homogeneous samples of hollow carbon nanospheres from cellulose chars. *J. Am. Chem. Soc.* **2003**, *125*, 9916–9917. [CrossRef] [PubMed]
38. Mani, R.C.; Li, X.; Sunkara, M.K.; Rajan, K. Carbon nanopipettes. *Nano Lett.* **2003**, *3*, 671–673. [CrossRef]
39. Qin, Y.; Jiang, X.; Cui, Z.L. Low-Temperature Synthesis of Amorphous Carbon Nanocoils via Acetylene Coupling on Copper Nanocrystal Surfaces at 468 K: A Reaction Mechanism Analysis. *J. Phys. Chem. B* **2005**, *109*, 21749–21754. [CrossRef] [PubMed]
40. Qin, Y.; Zhang, Z.K.; Cui, Z.L. Helical carbon nanofibers prepared by pyrolysis of acetylene with a catalyst derived from the decomposition of copper tartrate. *Carbon* **2003**, *41*, 3063–3074. [CrossRef]
41. Qin, Y.; Zhang, Z.K.; Cui, Z.L. Helical carbon nanofibers with a symmetric growth mode. *Carbon* **2004**, *42*, 1917–1922. [CrossRef]
42. Qin, Y.; Zhang, Q.; Cui, Z.L. Effect of synthesis method of nanocopper catalysts on the morphologies of carbon nanofibers prepared by catalytic decomposition of acetylene. *J. Catal.* **2004**, *223*, 389–394. [CrossRef]
43. Novoselov, K.S.; Geim, A.K.; Morozov, S.V.; Jiang, D.; Zhang, Y.; Dubonos, S.V.; Grigorieva, I.V.; Firsov, A.A. Electric field effect in atomically thin carbon films. *Science* **2004**, *306*, 666–669. [CrossRef] [PubMed]
44. Geim, A.K. Graphene: Status and prospects. *Science* **2005**, *324*, 1530–1534. [CrossRef] [PubMed]
45. Qi, X.S.; Xu, M.H.; Zhong, W.; Ye, X.J.; Deng, Y.; Au, C.T.; Jin, C.Q.; Du, Y.W. Magnetic properties and large-scale synthesis of novel carbon nanocomposites via benzene decomposition over Ni nanoparticles. *J. Phys. Chem. C* **2009**, *113*, 2267–2272. [CrossRef]
46. Qi, X.S.; Yang, Y.; Zhong, W.; Deng, Y.; Au, C.T.; Du, Y.W. Large-scale synthesis, characterization and microwave absorption properties of car bon nanotubes of different helicities. *J. Solid State Chem.* **2009**, *182*, 2691–2697. [CrossRef]
47. Qi, X.; Deng, Y.; Zhong, W.; Yang, Y.; Qin, C.; Au, C.; Du, Y. Controllable and Large-Scale Synthesis of Carbon Nanofibers, Bamboo-Like Nanotubes, and Chains of Nanospheres over Fe/SnO_2 and Their Microwave-Absorption Properties. *J. Phys. Chem. C* **2010**, *114*, 808–814. [CrossRef]
48. Shen, W.; Huggins, F.E.; Shah, N.; Jacobs, G.; Wang, Y.; Shi, X.; Huffman, G.P. Novel Fe-Ni nanoparticle catalyst for the production of CO- and CO_2-free H_2 and carbon nanotubes by dehydrogenation of methane. *Appl. Catal. A* **2008**, *351*, 102–110. [CrossRef]
49. Li, Z.; Chen, J.; Zhang, X.; Li, Y.; Fung, K. Catalytic synthesized carbon nanostructures from methane using nanocrystalline Ni. *Carbon* **2002**, *40*, 409–415. [CrossRef]
50. Allaedini, G.; Tasirin, S.M.; Aminayi, P.; Yaakob, Z.; Talib, M.Z.M. Bulk production of bamboo-shaped multi-walled carbon nanotubes via catalytic decomposition of methane over tri-metallic Ni–Co–Fe catalyst. *React. Kinet. Mech. Catal.* **2015**, *116*, 385–396. [CrossRef]
51. Li, Z.; Larsson, J.A.; Larsson, P.; Ahuja, R.; Tobin, J.M.; O'Byrne, J.; Morris, M.A.; Attard, G.; Holmes, J.D. Copper/Molybdenum Nanocomposite Particles as Catalysts for the Growth of Bamboo-Structured Carbon Nanotubes. *J. Phys. Chem. C* **2008**, *112*, 12201–12206. [CrossRef]
52. Nieto-Márquez, A.; Valverde, J.L.; Keane, M.A. Catalytic growth of structured carbon from chloro-hydrocarbons. *Appl. Catal. A* **2007**, *332*, 237–246. [CrossRef]
53. Inoue, M.; Asai, K.; Nagayasu, Y.; Takane, K.; Iwamoto, S.; Yagasaki, E.; Ishii, K. Formation of multi-walled carbon nanotubes by Ni-catalyzed decomposition of methane at 600–750 °C. *Diam. Relat. Mater.* **2008**, *17*, 1471–1475. [CrossRef]

54. Dębek, R.; Galvez, M.E.; Launay, F.; Motak, M.; Grzybek, T.; Costa, P.D. Low temperature dry methane reforming over Ce, Zr and CeZr promoted Ni-Mg-Al hydrotalcite derived catalysts. *Int. J. Hydrogen Energy* **2016**, *41*, 11616–11623. [CrossRef]
55. Siew, K.W.; Lee, H.C.; Khan, M.R.; Gimbun, J.; Cheng, C.K. CO_2 reforming of glycerol over La-Ni/Al_2O_3 catalyst: A longevity evaluative study. *J. Energy Chem.* **2015**, *24*, 366–373. [CrossRef]
56. Martin-Gullon, I.; Vera, J.; Conesa, J.A.; González, J.L.; Merino, C. Differences between carbon nanofibers produced using Fe and Ni catalysts in a floating catalyst reactor. *Carbon* **2006**, *44*, 1572–1580. [CrossRef]
57. González, I.; Jesus, J.D.; Canizales, E. Bamboo-shaped carbon nanotubes generated by methane thermal decomposition using Ni nanoparticles synthesized in water-oil emulsions. *Micron* **2011**, *42*, 819–825. [CrossRef] [PubMed]
58. Chen, J.; Li, Y.; Ma, Y.; Qin, Y.; Chang, L. Formation of bamboo-shaped carbon filaments and dependence of their morphology on catalyst composition and reaction conditions. *Carbon* **2001**, *39*, 1467–1475. [CrossRef]
59. Shen, Y.; Lua, A.C. Synthesis of Ni and Ni-Cu supported on carbon nanotubes for hydrogen and carbon production by catalytic decomposition of methane. *Appl. Catal. B* **2015**, *164*, 61–69. [CrossRef]
60. Velasquez, M.; Batiot-Dupeyrat, C.; Gallego, J.; Santamaria, A. Chemical and morphological characterization of multi-walled-carbon nanotubes synthesized by carbon deposition from an ethanol-glycerol blend. *Diam. Relat. Mater.* **2014**, *50*, 38–48. [CrossRef]
61. Wang, C.; Zhan, L.; Wang, Y.; Qiao, W.; Liang, X.; Ling, L. Effect of sulfur on the growth of carbon nanotubes by detonation-assisted chemical vapor deposition. *Appl. Surf. Sci.* **2010**, *257*, 932–936. [CrossRef]
62. Brown, B.; Parker, C.B.; Stoner, B.R.; Glass, J.T. Growth of vertically aligned bamboo-like carbon nanotubes from ammonia/methane precursors using a platinum catalyst. *Carbon* **2011**, *49*, 266–274. [CrossRef]
63. Erkiaga, A.; Lopez, G.; Amutio, M.; Bilbao, J.; Olazar, M. Syngas from steam gasification of polyethylene in a conical spouted bed reactor. *Fuel* **2013**, *109*, 461–469. [CrossRef]
64. Wu, C.; Williams, P.T. Pyrolysis–gasification of post-consumer municipal solid plastic waste for hydrogen production. *Int. J. Hydrogen Energy* **2010**, *35*, 949–957. [CrossRef]
65. Kaewpengkrow, P.; Atong, D.; Sricharoenchaikul, V. Pyrolysis and gasification of land filled plastic wastes with Ni–Mg–La/Al_2O_3 catalyst. *Environ. Technol.* **2012**, *33*, 2489–2495. [CrossRef] [PubMed]
66. Wilk, V.; Hofbauer, H. Conversion of mixed plastic wastes in a dual fluidized bed steam gasifier. *Fuel* **2013**, *107*, 787–799. [CrossRef]
67. Acomb, J.C.; Nahil, M.A.; Williams, P.T. Thermal processing of plastics from waste electrical and electronic equipment for hydrogen production. *J. Anal. Appl. Pyrolysis* **2013**, *103*, 320–327. [CrossRef]
68. Lee, J.W.; Yu, T.U.; Lee, J.W.; Moon, J.H.; Jeong, H.J.; Park, S.S.; Yang, W.; Lee, U.D. Gasification of mixed plastic wastes in a moving-grate gasifier and application of the producer gas to a power generation engine. *Energy Fuels* **2013**, *27*, 2092–2098. [CrossRef]
69. Wu, C.; Williams, P.T. Pyrolysis–gasification of plastics, mixed plastics and real-world plastic waste with and without Ni–Mg–Al catalyst. *Fuel* **2010**, *89*, 3022–3032. [CrossRef]
70. Nahil, M.A.; Wu, C.; Williams, P.T. Influence of metal addition to Ni-based catalysts for the co-production of carbon nanotubes and hydrogen from the thermal processing of waste polypropylene. *Fuel Process. Technol.* **2015**, *130*, 46–53. [CrossRef]
71. Acomb, J.C.; Wu, C.; Williams, P.T. The use of different metal catalysts for the simultaneous production of carbon nanotubes and hydrogen from pyrolysis of plastic feedstocks. *Appl. Catal. B* **2016**, *180*, 497–510. [CrossRef]
72. Wang, P.; Xiao, P.; Zhong, S.; Chen, J.; Lin, H.; Wu, X. Bamboo-like carbon nanotubes derived from colloidal polymer nanoplates for efficient removal of bisphenol A. *J. Mater. Chem. A* **2016**, *4*, 15450–15456. [CrossRef]
73. Wisniewski, M.; Terzyk, A.; Gauden, P.; Kaneko, K.; Hattori, Y. Removal of internal caps during hydrothermal treatment of bamboo-like carbon nanotubes and application of tubes in phenol adsorption. *J. Colloid Interface Sci.* **2012**, *381*, 36–42. [CrossRef] [PubMed]
74. Chen, L.; Xia, K.; Huang, L.; Li, L.; Pei, L.; Fei, S. Facile synthesis and hydrogen storage application of nitrogen-doped carbon nanotubes with bamboo-like structure. *Int. J. Hydrogen Energy* **2013**, *38*, 3297–3303. [CrossRef]
75. Xu, X.; Tan, H.; Xi, K.; Ding, S.; Yu, D.; Cheng, S.; Yang, G.; Peng, X.; Fakeeh, A.; Kumar, R. Bamboo-like amorphous carbon nanotubes clad in ultrathin nickel oxide nanosheets for lithium-ion battery electrodes with long cycle life. *Carbon* **2015**, *84*, 491–499. [CrossRef]

76. Primo, E.; Gutierrez, F.; Rubianes, M.; Rivas, G. Bamboo-like multiwalled carbon nanotubes dispersed in double stranded calf-thymus DNA as a new analytical platform for building layer-by-layer based biosensors. *Electrochim. Acta* **2015**, *182*, 391–397. [CrossRef]
77. Lv, H.L.; Liang, X.H.; Cheng, Y.; Zhang, H.Q.; Tang, D.M.; Zhang, B.S.; Ji, G.B.; Du, Y.W. Coin-like α-Fe_2O_3@$CoFe_2O_4$ core-Shell composites with excellent electromagnetic absorption performance. *ACS Appl. Mater. Interfaces* **2015**, *7*, 4744–4750. [CrossRef] [PubMed]
78. Kong, L.; Wang, C.; Yin, X.; Fan, X.; Wang, W.; Huang, J. Electromagnetic wave absorption properties of carbon nanotube modified by tetrapyridinoporphyrazine interface layer. *J. Mater. Chem. C* **2017**, *5*, 7479–7488. [CrossRef]
79. Wu, H.; Wu, G.; Ren, Y.; Li, X.; Wang, L. Multishelled metal oxide hollow spheres: Easy synthesis and formation mechanism. *Chem. Eur. J.* **2016**, *22*, 8864–8871. [CrossRef] [PubMed]
80. Qin, M.; Shuai, Q.; Wu, G.; Zheng, B.; Wang, Z.; Wu, H. Zinc ferrite composite material with controllable morphology and its applications. *Mater. Sci. Eng. B* **2017**, *224*, 125–138. [CrossRef]
81. Fan, Y.; Qiao, T.; Zhang, F.; Fu, Q.; Dong, J.; Kong, B.; Li, H. An electromagnetic modulator based on electrically controllable metamaterial analogue to electromagnetically induced transparency. *Sci. Rep.* **2017**, *7*, 40441. [CrossRef] [PubMed]
82. Fan, Y.; Shen, N.-H.; Zhang, F.; Wei, Z.; Li, H.; Zhao, Q.; Fu, Q.; Zhang, P.; Koschny, T.; Soukoulis, C.M. Electrically tunable Goos-Hänchen effect with graphene in the terahertz regime. *Adv. Opt. Mater.* **2016**, *4*, 1824–1828. [CrossRef]
83. Fan, Y.; Shen, N.-H.; Koschny, T.; Soukoulis, C.M. Tunable terahertz meta-surface with graphene cut-wires. *ACS Photonics* **2015**, *2*, 151–156. [CrossRef]
84. Feng, A.; Wu, G.; Pan, C.; Wang, Y. The behavior of acid treating carbon fiber and the mechanical properties and thermal conductivity of phenolic resin matrix composites. *J. Nanosci. Nanotechnol.* **2017**, *17*, 3786–3791. [CrossRef]
85. Feng, A.; Wu, G.; Pan, C.; Wang, Y. Synthesis, preparation and mechanical property of wood fiber-reinforced poly(vinyl chloride) composites. *J. Nanosci. Nanotechnol.* **2017**, *17*, 3859–3863. [CrossRef]
86. Gu, J.; Dong, W.; Tang, Y.; Guo, Y.; Tang, L.; Kong, J.; Tadakamalla, S.; Wang, B.; Guo, Z. Ultra-low dielectric, fluoride-containing cyanate ester resins combining with prominent mechanical properties and excellent thermal and dimension stabilities. *J. Mater. Chem. C* **2017**, *5*, 6929–6936. [CrossRef]
87. Gu, J.; Guo, Y.; Yang, X.; Liang, C.; Geng, W.; Tang, L.; Li, N.; Zhang, Q. Synergistic improvement of thermal conductivities of polyphenylene sulfide composites filled with boron nitride hybrid fillers. *Compos. Part A* **2017**, *95*, 267–273. [CrossRef]
88. Wu, H.; Wu, G.; Wu, Q.; Wang, L. Facile synthesis and microwave absorbability of C@Ni-NiO core-shell hybrid solid sphere and multi-shelled NiO Hollow sphere. *Mater. Charact.* **2014**, *97*, 18–26. [CrossRef]
89. Wu, H.; Wu, Q.; Wang, L. Design and wide range microwave absorption of porous Co-Co_3O_4 hybrid hollow sphere with magnetic multi-resonance mechanisms. *Mater. Charact.* **2015**, *103*, 1–10. [CrossRef]